Thermodynamic Geometry Through Second Order Phase Transitions

Omer M. Basri[1]

[1]*Department of Physics of Complex Systems,*

Weizmann Institute of Science, Rehovot 76100, Israel.

(Dated: December 11, 2025)

Abstract

Thermodynamic geometry provides a powerful framework to analyze the dissipation of physical systems driven out of equilibrium, but near equilibrium. In its original formulation, the system's relaxation timescales had to be, to good approximation, constant throughout the control parameter space. In its current form, the formalism requires that linear response theory holds. This thesis studies the thermodynamic geometry of systems that undergo second-order phase transitions.

Using the scaling hypothesis, which provides the form of the divergent part of the free energy across universality classes, I show that while the Ruppeiner metric diverges at the critical point, the thermodynamic length may remain finite. The dynamical scaling hypothesis relates the response time near a phase transition to the scaling of the free energy, allowing the divergence of the metric in the Sivak–Crooks formulation to be evaluated. This analysis shows that the thermodynamic length can diverge in some systems, but likely converges in higher-dimensional systems with Ising-like phase transitions, suggesting a critical dimensionality of three.

Finally, I compute the Sivak-Crooks metric of the mean-field antiferromagnetic Ising model, and use it to study optimal protocols connecting points of interest in the system. I show analytically that in the disordered phase, the metric effectively reduces to a 1D manifold, allowing for simple determination of optimal protocols. In the ordered phase, I numerically find optimal protocols using the Fast-Marching method.

CONTENTS

LIST OF ABBREVIATIONS

MF: Mean-Field

1D/2D/3D: One-, two-, or three-dimensional systems

I. INTRODUCTION

Since the earliest developments of thermodynamics, there have been attempts to cast the theory in geometric form [1]. A geometric interpretation exists for equilibrium thermodynamics—for instance, the work performed by a heat engine corresponds to the area enclosed by its stroke in the PV plane. However, an analogous geometric relation for excess dissipation in non-equilibrium processes remains elusive.

One approach that bridges this gap is thermodynamic geometry, introduced in the 1970s by Ruppeiner and Weinhold [2, 3]. In their formulation, the space of thermodynamic parameters is endowed with a Riemannian metric derived from the second derivatives of a thermodynamic potential—such as the internal energy, entropy, or any of their Legendre transforms. Although the choice of potential changes the explicit form of the metric, the resulting manifold remains invariant [4].

In the 1980s, Salamon [5] established a connection between excess dissipation and thermodynamic length in this Riemannian manifold, subject to two important limitations. First, the result holds only for endoreversible processes, where the system remains in internal equilibrium but may be out of equilibrium with its environment. Second, the dissipation depends explicitly on the mean response time of the system, restricting the formalism's applicability to systems with varying relaxation times. Despite these limitations, the framework has proven valuable for identifying minimal-entropy-production protocols in processes such as chemical reactions and distillation [6].

Building on this line of work, Sivak and Crooks [7, 8] derived a closely related metric using LRT (linear response theory). In their formulation, the system's relaxation dynamics are incorporated directly into the metric, thereby removing the dependence on a separate response-time parameter and eliminating the assumption of endoreversibility. This generalized framework extends thermodynamic geometry to a much broader class of systems—including those with widely varying time scales and microscopic systems such as biomolecular or single-molecule systems—and has found applications in optimizing computational and physical processes [9].

A particularly challenging class of systems exhibiting widely separated time scales are those undergoing phase transitions. The application of thermodynamic geometry to such systems has drawn significant attention [10, 11], including efforts to identify optimal driving protocols across critical regions (e.g., the 2D ferromagnetic Ising model [12]). Yet, the divergence of thermodynamic length near phase transitions has received limited study.

In systems with disconnected phases, any transformation from one phase to another must necessarily cross a phase transition. One such case, examined in this work, is the mean-field (MF) antiferromagnet, where the phase boundary entirely separates distinct thermodynamic phases. Determining whether the thermodynamic length remains finite near such transitions is crucial for understanding the applicability of thermodynamic geometry in these regimes.

Both the Ruppeiner and Sivak metrics predict that the thermodynamic metric should diverge in the vicinity of a second-order phase transition (see Sec. III). A natural question, therefore, is whether this divergence of the metric translates into a divergence of the corresponding thermodynamic lengths. Note that even if the length remains finite, other geometric quantities such as the curvature may diverge, signaling critical behavior. Though these do not directly contribute to dissipation and are thus outside our present focus.

In this thesis, I analyze the behavior of thermodynamic geometry near second-order phase transitions. I show that the Ruppeiner and Sivak manifolds exhibit qualitatively distinct behavior around criticality, primarily due to the phenomenon of critical slowing down. Interestingly, there exist cases where the metric does not diverge at the transition.

Finally, I calculate both the ruppiner and Sivak metrics for the MF antiferromagnet. Using the Sivak metric I determine the optimal protocol connecting point-pairs of interest. Because the two phases are entirely separated

by a phase boundary, any such protocol necessarily traverses a phase transition. My results show that, there are cases where the optimal path crosses the phase transition even when a path exists that avoids it.

II. GOALS

We wish to focus on the following questions:

- What happens to the dissipated availability when crossing a second order phase transition?
- Is it possible for the optimal path to traverse a second-order phase transition, even when an alternative path confined to a single phase is available?

Answering these questions can clarify how thermodynamic geometry can be applied to systems undergoing second-order phase transitions. This, in turn, will inform future optimization of driving protocols—indicating whether this approximate geometric framework may direct optimal paths through phase transitions, or whether alternative optimization approaches are required to handle protocols that cross phase boundaries.

III. FRAMEWORK

Before analyzing thermodynamic geometry near second-order phase transitions, a brief definition of the key metrics and scaling tools used in this study is appropriate.

A. Ruppeiner and Weinhold Metric

The Ruppeiner–Weinhold metric [2, 3] is defined as the Hessian of a thermodynamic potential or generalized entropy:

$$g^R_{\mu\nu} = \pm \frac{\partial^2 \varphi}{\partial \lambda^\mu \partial \lambda^\nu} \tag{1}$$

where φ is a thermodynamic potential (e.g., internal energy, entropy, or their Legendre transform), and λ^μ are its natural variables (e.g., $\{S, M\}$ – entropy and magnetization – for E). The sign ensures positive definiteness, consistent with the convexity or concavity of φ [13]. In the original works, these definitions were introduced without a specific physical motivation, but rather as a mathematical observation that they constitute a well-defined Riemannian metric.

Salamon [5] connected this metric to excess dissipation through the dissipated availability:

$$\mathcal{A}^R = \bar{\epsilon} \int_{\lambda(s)} g^R_{\mu\nu}\, \dot{\lambda}^\mu \dot{\lambda}^\nu \, ds \tag{2}$$

where $\bar{\epsilon}$ is the average response time. This result was derived under the endoreversible assumption, wherein the system is internally equilibrated at all times but not necessarily in equilibrium with its environment. The corresponding thermodynamic length is

$$\mathcal{L} = \int_{\lambda(s)} \sqrt{g^R_{\mu\nu}\, \dot{\lambda}^\mu \dot{\lambda}^\nu}\, ds \tag{3}$$

Minimizing $\mathcal{L}$ minimizes excess dissipation for a fixed-duration protocol, a result of the Cauchy–Schwarz inequality:

$$\mathcal{A}^R \geq \frac{\bar{\epsilon}}{\tau}\mathcal{L}^2 \tag{4}$$

with equality for constant-speed protocols (i.e $\sqrt{g_{\mu\nu}\, \dot{\lambda}^\mu \dot{\lambda}^\nu} = \text{const.}$).

B. Sivak and Crooks Metric

The assumptions of endoreversibility and uniform response times restrict the applicability of this formalism. Sivak and Crooks [7] lifted these limitations by employing linear-response theory, defining

$$g^S_{\mu\nu} = \int_0^\infty \langle \delta X_\mu(t)\, \delta X_\nu(0) \rangle\, dt = \mathcal{T}_{\mu\nu} \frac{\partial^2 \ln Z}{\partial \lambda^\mu \partial \lambda^\nu} \tag{5}$$

where $\mathcal{T}_{\mu\nu}$ is the time-response matrix, Z the partition function, and X_μ the conjugate variable to λ^μ. The response time is thus encoded directly in the metric, and the dissipated availability becomes

$$\mathcal{A}^S = \int_{\lambda(t)} g^S_{\mu\nu}\, \dot{\lambda}^\mu \dot{\lambda}^\nu\, dt \tag{6}$$

The thermodynamic length in this formalism retains the same definition, just using the new metric definition:

$$\mathcal{L} = \int_{\lambda(s)} \sqrt{g^S_{\mu\nu}\, \dot{\lambda}^\mu \dot{\lambda}^\nu}\, ds \tag{7}$$

with the inequality

$$\mathcal{A}^S \geq \frac{\mathcal{L}^2}{\tau} \tag{8}$$

again saturated by constant-speed protocols.

C. Scaling Hypothesis

Near second order phase transitions, derivatives of the free energy – and hence the Ruppeiner and Sivak metrics often diverge (for example, via diverging magnetic susceptibility). Although exact partition functions are rarely tractable, the asymptotic form of these divergences is determined by critical exponents defining universality classes.

The scaling hypothesis connects the divergent part of the free energy near the critical point to a set of reduced variables. For Ising-type models, the critical point is some (T_c, H_c), the reduced variables are defined as $t = (T - T_c)/T_c$ and $h = (H - H_c)/H_c$, and the singular contribution to the free energy scales as

$$\varphi \propto t^b f\left(\frac{h}{t^\Delta}\right), \tag{9}$$

where $f(x)$ is continuous and satisfies $f(x) \sim x^p$ as $x \to \infty$ [14]. The exponents b, Δ, and p are determined by the standard critical exponents—for example, $b = 2 - \alpha$, where α is the heat-capacity exponent. For models with different symmetries, the definitions of the reduced variables and the precise form of the scaling relation may differ. While this framework effectively captures metric divergences across universality classes, it does not account for relaxation times, which influence dissipation through the mean relaxation time $\bar{\epsilon}$ in the Ruppeiner formalism, and affect both the thermodynamic length and dissipation in the Sivak formulation.

Dynamic Scaling Hypothesis

Critical slowing down near second-order transitions leads to divergent relaxation times. The dynamic scaling hypothesis relates the relaxation time τ and correlation length ξ as [15]

$$\tau \propto \xi^z \tag{10}$$

and the free energy scales as $\varphi \propto \xi^{-d}$ [14]. Combining these yields

$$\tau \propto \varphi^{-z/d} \propto t^{-bz/d}\, f^{-z/d}\left(\frac{h}{t^\Delta}\right) \tag{11}$$

linking dynamical and thermodynamic critical behavior.

D. Divergence of Lengths

A diverging metric does not necessarily imply a divergent thermodynamic length – analogous to how the Schwarzschild metric diverges at $r = r_s$ without a corresponding geometric singularity. For constant-speed protocols of fixed duration,

$$\mathcal{A} \propto \mathcal{L}^2 \tag{12}$$

Thus, a finite thermodynamic length guarantees the existence of a finite-dissipation protocol. As opposed to that, from the Cauchy-Schwarz inequality $\mathcal{L} \to \infty$ implies $\mathcal{A} \to \infty$.

Consequently, the convergence of thermodynamic length determines whether finite-dissipation protocols exist. If $\ell(s) = \sqrt{g_{\mu\nu}\dot{\lambda}^\mu(s)\,\dot{\lambda}^\nu(s)} \propto s^{-p}$ near criticality (as $s \to 0$), the total length diverges only for $p > 1$.

Note that this observation does not necessarily inform us about the metric itself, or intrinsic geometry of the manifold. The metric might diverge for flat space [16, 17], and the manifold might have divergent curvature despite having finite lengths and a non-divergent metric.

IV. RESULTS

A. Scaling Hypothesis

1. *Scaling Hypothesis for the Free Energy*

We employ the scaling hypothesis for the free energy to analyze the divergence of the Ruppeiner metric and determine whether the thermodynamic length diverges along paths crossing a phase transition.

Assuming the singular part of the thermodynamic potential potential scales as

$$\varphi \propto t^b f\left(\frac{h}{t^\Delta}\right) \tag{13}$$

the metric near criticality $(t, h \to 0)$ scales as

$$\left(g_{\mu\nu}\right)\Big|_{\frac{h}{t^\Delta}\to\text{const.}} \propto \begin{pmatrix} t^{b-2} & t^{b-\Delta-1} \\ t^{b-\Delta-1} & t^{b-2\Delta} \end{pmatrix}, \tag{14}$$

$$\left(g_{\mu\nu}\right)\Big|_{\frac{h}{t^\Delta}\to\infty} \propto \begin{pmatrix} t^{-2}h^p & t^{-1}h^{p-1} \\ t^{-1}h^{p-1} & h^{p-2} \end{pmatrix}. \tag{15}$$

Here, the two limits correspond to different asymptotic behaviors of f as $\frac{h}{t^\Delta}$ tends to a constant or diverges.

To study length divergences, we must specify the path in parameter space, which determines the scaling of $\frac{h}{t^\Delta}$. We consider two representative cases.

a. Case 1: $\frac{h}{t^\Delta} \to const.$

$$\begin{pmatrix} t \\ h \end{pmatrix} = \begin{pmatrix} s \\ s^k \end{pmatrix}, \quad k \geq \Delta \tag{16}$$

for which

$$\frac{h}{t^\Delta} \xrightarrow[s\to 0]{} \text{const.}$$

The metric contributions then scale as

$$g_{tt}\dot{t}^2 \propto s^{b-2} \qquad g_{th}\dot{t}\dot{h} \propto s^{b-2+(k-\Delta)} \qquad g_{hh}\dot{h}^2 \propto s^{b-2+2(k-\Delta)}$$

Since $k \geq \Delta$, the sufficient condition for convergence of the Ruppeiner length $\mathcal{L}$ is

$$b > 0 \tag{17}$$

As established earlier, convergence of $\mathcal{L}$ is necessary and sufficient for convergence of the Salamon dissipated availability $\mathcal{A}$ in finite-time protocols, provided $\bar{\epsilon}$ remains finite.

b. Case 2: $\frac{h}{t^\Delta} \to \infty$

$$\begin{pmatrix} t \\ h \end{pmatrix} = \begin{pmatrix} s^{1/k} \\ s \end{pmatrix}, \quad k < \Delta \tag{18}$$

implying

$$\frac{h}{t^\Delta} \xrightarrow[s\to 0]{} \infty$$

In this case,

$$g_{tt}\,\dot{t}^2 \propto s^{p-2} \qquad g_{th}\,\dot{t}\,\dot{h} \propto s^{p-2} \qquad g_{hh}\,\dot{h}^2 \propto s^{p-2}$$

Hence, convergence requires

$$p > 0 \tag{19}$$

Both conditions ($b > 0$ and $p > 0$) hold for several universality classes, as shown in Table I.

	b	p
Mean Field	2	$\frac{4}{3}$
2D Ising	2	$\frac{16}{15}$
3D Ising	1.8899(3)	1.2088(1)
2D 3-state Potts	$\frac{5}{3}$	$\frac{15}{14}$
2D 4-state Potts	$\frac{4}{3}$	$\frac{16}{15}$

TABLE I: Scaling parameters for representative universality classes.

2. *Dynamical Scaling Hypothesis*

In both Ruppeiner and Sivak formalisms, dissipation depends on the system's response time – appearing as $\bar{\epsilon}$ in the former and directly in the metric for the latter. Using the dynamical scaling hypothesis, we can study how the relaxation time τ diverges.

From $\tau \propto \psi^{-z/d}$ and the static scaling relation, we obtain

$$\tau \propto t^{-bz/d}\, w\left(\frac{h}{t^\Delta}\right) \tag{20}$$

where $w(x)$ is continuous and satisfies

$$w(x) \xrightarrow[x\to\infty]{} x^{-pz/d} \tag{21}$$

Hence, the divergence of τ follows

$$\tau \propto \begin{cases} t^{-bz/d}, & \frac{h}{t^\Delta} \to \text{const.} \\ h^{-pz/d}, & \frac{h}{t^\Delta} \to \infty \end{cases} \tag{22}$$

Including this factor modifies the scaling of the metric elements in Case 1

$$g_{tt}\,\dot{t}^2 \propto s^{b(1-z/d)-2} \tag{23}$$

$$g_{th}\,\dot{t}\,\dot{h} \propto s^{b(1-z/d)-2+(k-\Delta)} \tag{24}$$

$$g_{hh}\,\dot{h}^2 \propto s^{b(1-z/d)-2+2(k-\Delta)} \tag{25}$$

Thus, the convergence condition becomes

$$b\left(1-\frac{z}{d}\right) > 0 \tag{26}$$

Similarly, in Case 2

$$g_{ij}\dot{\lambda}^i\dot{\lambda}^j \propto s^{p(1-z/d)-2} \tag{27}$$

so convergence requires

$$p\left(1-\frac{z}{d}\right) > 0 \tag{28}$$

As summarized in Table II, the thermodynamic lengths diverge for the 2D Ising and 2D Potts models but remain finite for the 3D Ising model. This, and RG results for the dynamical scaling hypothesis [18, 19], leads us to the conclusion that there is likely a critical dimension of 3 for convergence of the thermodynamic length.

	d	z	z/d
2D Ising	2	2.165(10)	1.083(5)
3D Ising	3	2.032(4)	0.677(1)
2D 3-state Potts	2	2.198(2)	1.099(1)
2D 4-state Potts	2	2.290(3)	1.095(2)

TABLE II: Dynamical scaling parameters for representative universality classes [20].

B. Antiferromagnetic Mean-Field Model - Ruppiner metric

As discussed earlier, the model used as a case study is the mean-field (MF) Ising model with antiferromagnetic interactions and a uniform magnetic field, in contrast to other treatments of antiferromagnets that introduce a staggered magnetic field acting oppositely on neighboring spins. In this model, it is impossible to construct a continuous path connecting the antiferromagnetic and disordered phases without crossing a second-order phase transition. This property makes it an ideal test case for applying the thermodynamic geometry framework laid out above.

I now show a calculation of the Ruppiner metric as well as an interesting result concerning minimal paths in the disordered phase, that turns out to be a general result for MF models.

1. The Model

We consider the MF antiferromagnet introduced by Vives *et al.* [21]. The system consists of spins arranged on a square lattice divided into two interpenetrating sublattices, A and B, such that spins on one sublattice interact only with spins on the other. Denoting the sublattice magnetizations by m_A and m_B, the Gibbs free energy per spin is

$$f = \frac{1}{2}\left[Km_Am_B - h\,(m_A + m_B) + \frac{1}{2}T\,(\vartheta(m_A) + \vartheta(m_B))\right] \tag{29}$$

where

$$\vartheta(x) = \frac{1}{2}[(1+x)\log(1+x) + (1-x)\log(1-x)] \tag{30}$$

and K is the product of the exchange interaction J and the coordination number.

At thermodynamic equilibrium, m_A and m_B minimize f and satisfy the self-consistency relations

$$m_A = \tanh\left(\frac{h - Km_B}{T}\right) \tag{31}$$

$$m_B = \tanh\left(\frac{h - Km_A}{T}\right) \tag{32}$$

Differentiating the Gibbs free energy with respect to T and h yields the Ruppeiner metric components:

$$g_{hh} = \frac{T(2 - m_A^2 - m_B^2) - 2K(1 - m_A^2)(1 - m_B^2)}{2\left[T^2 - K^2(1 - m_A^2)(1 - m_B^2)\right]} \tag{33}$$

$$g_{hT} = -\frac{(1 - m_A^2)\text{arctanh}(m_A)\left[T - K(1 - m_B^2)\right] + (1 - m_B^2)\text{arctanh}(m_B)\left[T - K(1 - m_A^2)\right]}{2\left[T^2 - K^2(1 - m_A^2)(1 - m_B^2)\right]} \tag{34}$$

$$g_{TT} = \frac{T\left[\text{arctanh}^2(m_A)(1 - m_A^2) + \text{arctanh}^2(m_B)(1 - m_B^2)\right] - K(1 - m_A^2)(1 - m_B^2)\text{arctanh}(m_A)\text{arctanh}(m_B)}{2\left[T^2 - K^2(1 - m_A^2)(1 - m_B^2)\right]} \tag{35}$$

2. Disordered Phase

In the disordered phase, the two sublattices become equivalent, $m_A = m_B \equiv m$. A notable property of the Ruppeiner metric in this regime is that its determinant vanishes, $g = 0$. This degeneracy, also observed in the ferromagnetic MF model [10], implies that one eigenvalue of the metric is zero. The corresponding null eigenvector aligns with directions of constant magnetization (equivalently, constant m_A, m_B). Consequently, motion along these directions incurs zero thermodynamic length, and the problem reduces effectively to a one-dimensional minimization: at what distance from the critical line is the thermodynamic length minimal? As shown below, the minimum occurs precisely on the phase transition line itself.

For clarity, we denote by T_c the critical temperature corresponding to a given magnetization. From differentiation of the free energy, two key relations follow along the phase transition line:

$$m_A = m_B = m \equiv \pm\sqrt{1 - \frac{T_c}{K}} \tag{36}$$

and

$$h_c(T_c) = \pm\left[K\sqrt{1 - \frac{T_c}{K}} + T_c \operatorname{arctanh}\left(\sqrt{1 - \frac{T_c}{K}}\right)\right] \tag{37}$$

In the disordered phase ($m_A = m_B = m$), the Ruppeiner metric simplifies to

$$g_{ij} = \frac{T_c}{K(T + T_c)} \begin{pmatrix} \operatorname{arctanh}^2(m) & -\operatorname{arctanh}(m) \\ -\operatorname{arctanh}(m) & 1 \end{pmatrix} \tag{38}$$

Its eigenvalues and eigenvectors are

$$\lambda_1 = 0, \quad \boldsymbol{v}_1 = \begin{pmatrix} 1 \\ \operatorname{arctanh}(m) \end{pmatrix} \tag{39}$$

$$\lambda_2 = 1 + \operatorname{arctanh}^2(m), \quad \boldsymbol{v}_2 = \begin{pmatrix} \operatorname{arctanh}(m) \\ -1 \end{pmatrix} \tag{40}$$

The null direction $\boldsymbol{v}_1$ defines "zero-length" lines, corresponding to constant-m curves in the (T, h) plane (see Fig. 1).

To find the minimal thermodynamic length, we consider displacements along the $\boldsymbol{v}_1$ direction. Since $g_{\mu\nu}$ scales as $(T + T_c)^{-1}$, while the differential displacement scales as the Euclidean distance projected onto the normal of the constant-magnetization lines, the relevant scaling is determined by the distance between neighboring constant-m curves.

Geometrically, this "radial distance" is proportional to a displacement along the T-axis, with some offset T_0 – since the constant-m lines are neither vertical nor horizontal except at symmetry points. Let (T_c, h_c) denote a point on the phase transition line and $(T_c + \delta_T,\ h_c + \frac{\partial h_c}{\partial T_c}\delta_T)$ a neighboring point. The intersection of the two constant-m lines can be expressed as

$$\begin{pmatrix} T_0 \\ h_0 \end{pmatrix} = a\,\boldsymbol{v}_1(T_c) + \begin{pmatrix} T_c \\ h_c \end{pmatrix} \tag{41}$$

$$\begin{pmatrix} T_0 \\ h_0 \end{pmatrix} = b\,\boldsymbol{v}_1(T_c + \delta_T) + \begin{pmatrix} T_c + \delta_T \\ h_c + \frac{\partial h_c}{\partial T_c}\delta_T \end{pmatrix} \tag{42}$$

Subtracting Eqs. (41)–(42) gives

$$\delta_T \begin{pmatrix} 1 \\ \frac{\partial h_c}{\partial T_c} \end{pmatrix} = \begin{pmatrix} 1 & 1 \\ \operatorname{arctanh}[m(T_c + \delta_T)] & \operatorname{arctanh}[m(T_c)] \end{pmatrix} \begin{pmatrix} -b \\ a \end{pmatrix} \tag{43}$$

Inverting this matrix yields

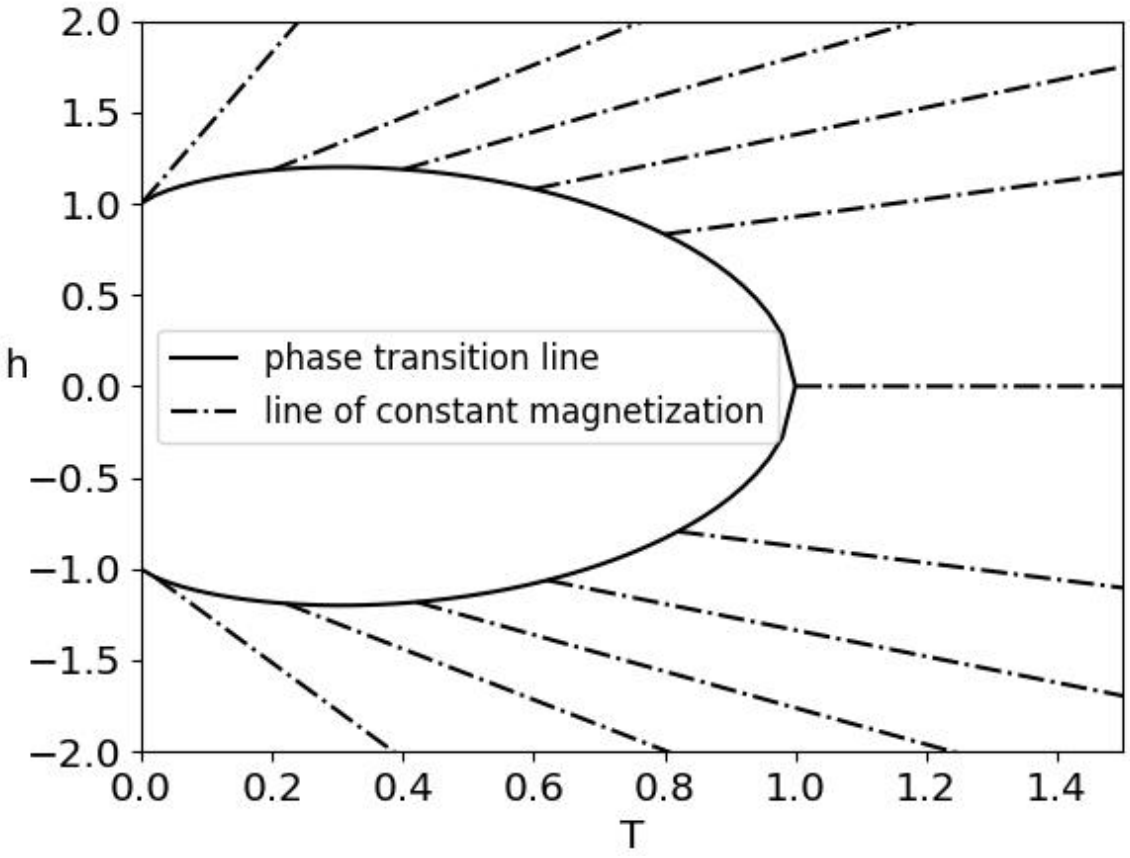

FIG. 1: Lines of zero thermodynamic length ($\lambda_1 = 0$) in the disordered phase.

$$\begin{pmatrix} 1 & 1 \\ \operatorname{arctanh}[m(T_c+\delta_T)] & \operatorname{arctanh}[m(T_c)] \end{pmatrix}^{-1} = \frac{1}{\operatorname{arctanh}[m(T_c)] - \operatorname{arctanh}[m(T_c+\delta_T)]} \begin{pmatrix} \operatorname{arctanh}[m(T_c)] & -1 \\ -\operatorname{arctanh}[m(T_c+\delta_T)] & 1 \end{pmatrix}$$
$$\simeq -\frac{2T_c\sqrt{1-\frac{T_c}{K}}}{K\,\delta_T} \begin{pmatrix} \operatorname{arctanh}\sqrt{1-\frac{T_c}{K}} & -1 \\ -\operatorname{arctanh}\sqrt{1-\frac{T_c+\delta_T}{K}} & 1 \end{pmatrix} \tag{44}$$

Solving for a gives

$$a = \frac{2T_c}{K}\left[\operatorname{arctanh}\sqrt{1-\frac{T_c}{K}} - \frac{\partial h_c}{\partial T_c}\sqrt{1-\frac{T_c}{K}}\right] \tag{45}$$

Differentiating Eq. (37) yields

$$\frac{\partial h_c}{\partial T_c} = -\frac{1}{\sqrt{1-\frac{T_c}{K}}} + \operatorname{arctanh}\sqrt{1-\frac{T_c}{K}} \tag{46}$$

Substituting this into Eq. (45) gives a remarkably simple result:

$$a = \frac{2T_c}{K} \tag{47}$$

Substituting back into Eq. (41) yields

$$T_0 = T_c + \frac{2T_c}{K} = T_c \, \frac{K+2}{K} \tag{48}$$

Thus, the differential thermodynamic length between two neighboring constant-magnetization lines in the disordered phase scales as

$$\frac{(T + \frac{K+2}{K} T_c)^2}{T + T_c} \tag{49}$$

which attains its minimum at $T = T_c$. Therefore, the least-dissipation path in the disordered phase lies precisely along the phase transition line.

C. Antiferromagnetic Mean-Field Model - Sivak metric

We now determine the least-dissipation path between two states $(T_1, h_1) \to (T_2, h_2)$, with (T_1, h_1) in the antiferromagnetic phase and (T_2, h_2) in the disordered phase. In particular, we compute the Sivak metric for the MF antiferromagnetic model of [21].

1. The Model

The Massieu potential is

$$\psi \;= \ln Z = \; -\frac{1}{2}\Big[\beta K \, m_A m_B \;-\; \beta h \, (m_A + m_B) \;+\; \frac{1}{2}\left(\vartheta(m_A) + \vartheta(m_B)\right)\Big] \tag{50}$$

where $\beta = 1/T$.

2. Calculation of the Metric

The computation proceeds in three steps:

1. **Equilibrium covariances:** evaluate $\langle \delta m_i(0) \, \delta m_j(0) \rangle$ $(i, j \in \{A, B\})$.

2. **Dynamics and time integral:** incorporate linearized relaxation to obtain the integrated correlation.

3. **Variable transform:** convert to the $\boldsymbol{\lambda} = (\beta, \beta h) \equiv (\beta, \alpha)$ representation, which is the representation of our control parameters, via the Jacobian from (m_A, m_B) to $(-E, m)$.

Note we set $\alpha \equiv \beta h$ for brevity.

Let $\zeta_i \equiv 1 - m_i^2$ for $i \in \{A, B\}$. The inverse covariance is the Hessian of ψ with respect to (m_A, m_B):

$$-\Sigma^{-1} \;=\; \frac{1}{2}\begin{pmatrix} \dfrac{1}{\zeta_A} & \beta K \\ \beta K & \dfrac{1}{\zeta_B} \end{pmatrix}. \tag{51}$$

Its inverse is

$$\Sigma \;=\; \frac{2}{1 - \beta^2 K^2 \zeta_A \zeta_B} \begin{pmatrix} \zeta_A & -\beta K\, \zeta_A \zeta_B \\ -\beta K\, \zeta_A \zeta_B & \zeta_B \end{pmatrix} \tag{52}$$

The relaxation dynamics [22] are

$$\dot{m}_A = \Gamma[\tanh(\alpha - \beta K\, m_B) - m_A] \tag{53}$$

$$\dot{m}_B = \Gamma[\tanh(\alpha - \beta K\, m_A) - m_B] \tag{54}$$

with microscopic attempt rate Γ. Linearizing about equilibrium gives

$$\delta\dot{m}_A = \Gamma\,(-\,\delta m_A \;-\; \beta K\, \zeta_A\, \delta m_B) \tag{55}$$

$$\delta\dot{m}_B = \Gamma\,(-\,\beta K\, \zeta_B\, \delta m_A \;-\; \delta m_B) \tag{56}$$

In vector form, with $y = (\delta m_A, \delta m_B)^\top$

$$\dot{y} \;=\; -\Gamma \begin{pmatrix} 1 & \beta K\, \zeta_A \\ \beta K\, \zeta_B & 1 \end{pmatrix} y \;=\; -My \tag{57}$$

We require

$$\beta \int_0^\infty \langle \delta m_i(0)\, \delta m_j(t) \rangle\, dt \;=\; \beta \int_0^\infty \langle y(0)\, y^\top(t) \rangle\, dt \tag{58}$$

Since $\langle \delta m_i(0)\, \eta(t) \rangle = 0$ for $t > 0$, substituting $y(t) = e^{-Mt} y(0)$ yields

$$\begin{aligned} \beta \int_0^\infty \langle y(0)\, y^\top(t) \rangle\, dt = \beta\, \langle y(0)\, y^\top(0) \rangle \int_0^\infty e^{-M^\top t}\, dt \;&=\; \beta\, \Sigma\, (M^\top)^{-1} \\ &= \frac{2\beta}{\Gamma\big(1 - \beta^2 K^2 \zeta_A \zeta_B\big)^2} \begin{pmatrix} \zeta_A\big(1 + \beta^2 K^2 \zeta_A \zeta_B\big) & -2\beta K\, \zeta_A \zeta_B \\ -2\beta K\, \zeta_A \zeta_B & \zeta_B\big(1 + \beta^2 K^2 \zeta_A \zeta_B\big) \end{pmatrix} \end{aligned} \tag{59}$$

To express the Sivak metric in the control variables $\boldsymbol{\lambda} = (\beta, \alpha)$, we transform fluctuations to $(-E, m)$ via

$$E = \tfrac{1}{2} K\, m_A m_B \tag{60}$$

$$m = \tfrac{1}{2}(m_A + m_B) \tag{61}$$

so the Jacobian is

$$P \;=\; \frac{\partial(-E, m)}{\partial(m_A, m_B)} \;=\; \frac{1}{2}\begin{pmatrix} -K m_B & -K m_A \\ 1 & 1 \end{pmatrix} \tag{62}$$

The Sivak metric then reads

$$
\begin{aligned}
g_{\mu\nu}^{\text{Sivak}} &= \beta\, P\, \Sigma\, (M^{\top})^{-1} P^{\top} \\
&= \frac{\beta}{2\Gamma\left(1-\beta^2 K^2 \zeta_A \zeta_B\right)^2}
\begin{pmatrix}
K^2\Big[\left(1+\beta^2K^2\zeta_A\zeta_B\right)\left(m_A^2\zeta_B+m_B^2\zeta_A\right)-4\beta K\, m_A m_B \zeta_A\zeta_B\Big] & -K\Big[\left(1+\beta^2K^2\zeta_A\zeta_B\right)\left(m_A\zeta_B+m_B\zeta_A\right)-2\beta K(m_A+m_B)\zeta_A\zeta_B\Big] \\
-K\Big[\left(1+\beta^2K^2\zeta_A\zeta_B\right)\left(m_A\zeta_B+m_B\zeta_A\right)-2\beta K(m_A+m_B)\zeta_A\zeta_B\Big] & \left(1+\beta^2K^2\zeta_A\zeta_B\right)(\zeta_A+\zeta_B)-4\beta K\,\zeta_A\zeta_B
\end{pmatrix}
\end{aligned}
\tag{63}
$$

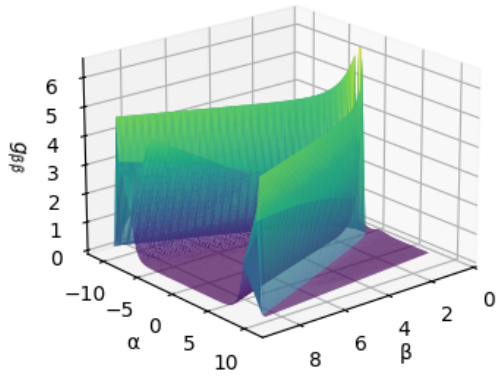

(a) Caloric element $g_{\beta\beta}$

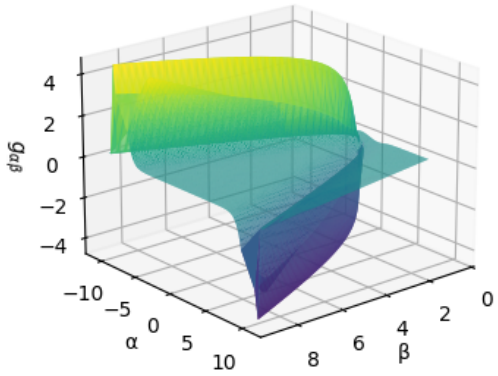

(b) Magneto–caloric element $g_{\alpha\beta}$

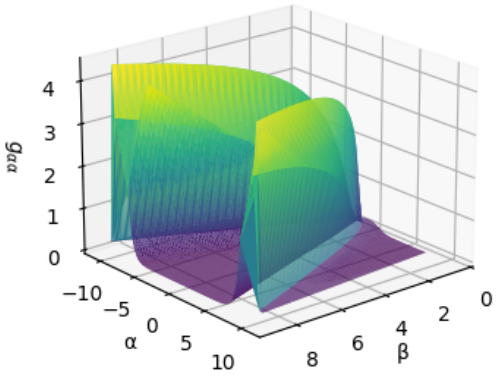

(c) Magnetic element $g_{\alpha\alpha}$

FIG. 2: Elements of the Sivak metric for the MF antiferromagnet

Figures 2 show the resulting metric components.

3. Disordered phase

It is convenient to define the total and staggered magnetizations

$$m = \frac{m_A + m_B}{2} \tag{64}$$

$$s = \frac{m_A - m_B}{2} \tag{65}$$

For each $m \in [-1, 1]$, the corresponding critical parameters (β_c, α_c) on the phase boundary satisfy

$$m = \pm\sqrt{1 - \frac{1}{\beta_c K}} \tag{66}$$

$$\alpha_c = \pm\Big(\beta_c K\, m + \operatorname{arctanh} m\Big) \tag{67}$$

In the disordered phase, $m_A = m_B \equiv m$ (hence $\zeta_A = \zeta_B \equiv \zeta$). The metric in this case reduces to

$$g_{\mu\nu} \;=\; \frac{\beta\,\zeta}{\Gamma\big(1 + \beta K \zeta\big)^2} \begin{pmatrix} K^2 m^2 & -Km \\ -Km & 1 \end{pmatrix}. \tag{68}$$

As in the ruppiner case, the metric is rank-one, with the null eigenvector aligning with directions of constant m. The problem of minimizing distances again reduces to a 1D minimization: at what distance from the phase boundary does the length become minimal? This will be calculated in the following paragraphs:

For each $m \in [-1, 1]$, the corresponding critical parameters (β_c, α_c) on the phase boundary satisfy

$$m = \pm\sqrt{1 - \frac{1}{\beta_c K}} \tag{69}$$

$$\alpha_c = \pm\Big(\beta_c K\, m + \operatorname{arctanh} m\Big) \tag{70}$$

The eigenpairs of the metric 68 are

$$\lambda_1 = 0 \quad : \qquad \boldsymbol{v}_1 = \begin{pmatrix} 1 \\ Km \end{pmatrix} \tag{71}$$

$$\lambda_2 = 1 + K^2 m^2 \quad : \qquad \boldsymbol{v}_2 = \begin{pmatrix} Km \\ -1 \end{pmatrix} \tag{72}$$

Thus the zero mode $\boldsymbol{v}_1$ follows lines of constant m in (β, α).

a. Scaling of the metric prefactor. From (69) we have $\zeta = 1 - m^2 = 1/(\beta_c K)$ along the phase boundary labeled by magnetization m, with critical parameter β_c. Using this in the prefactor gives

$$g_{\mu\nu} \;\propto\; \frac{\beta}{(\beta_c + \beta)^2}\,\big(1 + K^2 m^2\big). \tag{73}$$

b. Scaling of the displacement along the zero mode. Consider two neighboring constant-m lines labeled by $(\beta_{c1}, \alpha_{c1})$ and $(\beta_{c2}, \alpha_{c2}) = (\beta_{c1} + \delta_\beta, \alpha_{c1} + \delta_\alpha)$. We find their intersection with a straight line parallel to the zero mode at each point:

$$\begin{pmatrix}\beta\\ \alpha\end{pmatrix} = a\,\boldsymbol{v}_1(\beta_{c1}) + \begin{pmatrix}\beta_{c1}\\ \alpha_{c1}\end{pmatrix} \tag{74}$$

$$\begin{pmatrix}\beta\\ \alpha\end{pmatrix} = b\,\boldsymbol{v}_1(\beta_{c2}) + \begin{pmatrix}\beta_{c1} + \delta_\beta\\ \alpha_{c1} + \dfrac{\partial \alpha_c}{\partial \beta_c}\,\delta_\beta\end{pmatrix} \tag{75}$$

Subtracting (74) from (75) yields

$$\delta_\beta \begin{pmatrix}1\\ \dfrac{\partial \alpha_c}{\partial \beta_c}\end{pmatrix} = \begin{pmatrix}1 & 1\\ Km_2 & Km_1\end{pmatrix}\begin{pmatrix}-b\\ a\end{pmatrix} \tag{76}$$

where $m_1 = m(\beta_{c1})$, $m_2 = m(\beta_{c2})$. From (70) we have $\dfrac{\partial \alpha_c}{\partial \beta_c} = \dfrac{1}{m}$ Inverting gives

$$\begin{aligned} a &= \frac{1-m^2}{Km}\,\frac{\partial m}{\partial \beta_c} = \frac{1-m^2}{Km}\,\frac{2m}{(1-m^2)^2} \\ &= \frac{2}{K(1-m^2)} = 2\beta_c \end{aligned} \tag{77}$$

where we used $1 - m^2 = 1/(\beta_c K)$ and $\dfrac{\partial m}{\partial \beta_c} = \dfrac{2m}{(1-m^2)^2}$ from (69). Hence the displacement along the zero mode scales as $\delta\boldsymbol{\lambda} \sim (\beta + \beta_c)$.

c. Conclusion: minimum at $\beta = 0$. Combining the prefactor and displacement scalings,

$$\sqrt{\delta\lambda^\mu\, g_{\mu\nu}\, \delta\lambda^\nu} \;\propto\; \sqrt{\beta}$$

so the infinitesimal thermodynamic length is minimized at $\beta = 0$ (infinite temperature). Therefore, the optimal trajectory between two points in this phase follows the null direction (of constant magnetization) from the initial point to $\beta = 0$, then traverse along $\beta = 0$, then return along a null trajectory to the final point.

This is opposite to our result for the Ruppiner metric, where the optimal trajectory is along the phase transition line. Meaning, taking into account the divergence in response time substantially changes the optimal trajectory in this model.

4. Divergence at the Phase transition

In the ordered phase, near the critical line, the sublattice magnetizations can be expanded as shown in [21]:

$$m \approx \pm\sqrt{1 - \frac{1}{\beta_c K}} + a_m\,\Delta\alpha - b_m\,\Delta\beta \tag{78}$$

$$s \approx \sqrt{a_s\,\Delta\alpha + b_s\,\Delta\beta} \tag{79}$$

where $a_m, b_m, a_s, b_s > 0$, and

$$\Delta\alpha = \alpha - \alpha_c \qquad\qquad \Delta\beta = \beta - \beta_c$$

For brevity we define

$$\Delta_m = a_m\,\Delta\alpha - b_m\,\Delta\beta \qquad\qquad \Delta_s = a_s\,\Delta\alpha + b_s\,\Delta\beta$$

To lowest order in these small deviations, the sublattice magnetizations and corresponding susceptibilities satisfy

$$m_{A,B} \approx \pm\sqrt{1 - \frac{1}{\beta_c K}} \;\pm\; \sqrt{\Delta_s} \tag{80}$$

$$\zeta_{A,B} \approx \frac{1}{\beta_c K}\left(1 \pm 2\sqrt{\Delta_s}\right) \tag{81}$$

Substituting these expressions into the Sivak metric yields, to leading order,

$$g_{\mu\nu} \;\propto\; \Delta_s^{-1}$$

Hence, while the metric diverges as $\Delta_s \to 0$, the associated thermodynamic length remains finite.

5. *Minimal Paths*

We identify three distinct classes of minimal (shortest) paths, two of which cross the phase transition line.

Type A: Crossing between phases. In the first case, the initial and final states lie in different phases. The optimal trajectory proceeds from the initial point in the antiferromagnetic phase to the nearest point on the phase transition line, crosses into the disordered phase, and then ascends to infinite temperature ($\beta = 0$). Once at $\beta = 0$, the system moves horizontally along this line—where the thermodynamic length vanishes—until reaching the final magnetization, and finally descends along the constant-magnetization line to the destination point.

Type B: Crossing and returning. The second case occurs when both endpoints are in the antiferromagnetic phase, but it is shorter to cross the phase transition than to remain entirely within the ordered region. This trajectory can be viewed as a composition of two Type I paths: the system transitions from the ordered phase to the disordered phase and then back again. Because, as shown in Sec. IV C 3, paths within the disordered phase have zero thermodynamic length, the total length of such a trajectory is dominated by the two crossings.

Type C: Entirely within one phase. In the third case, both points are again in the same phase. Either in the disordered phase or in the antiferromagnetic phase. In the disordered case, the path will be composed of moving along the constant magnetization line to infinite temperature, along infinite temperature to the new

magnetization and back along the constant magnetization line. In the antiferromagnetic case, when the direct geodesic connecting the two points is shorter than any path that detours through the disordered region, the minimal path lies entirely within the ordered phase.

An illustration of these three classes of paths is shown in Fig. 3.

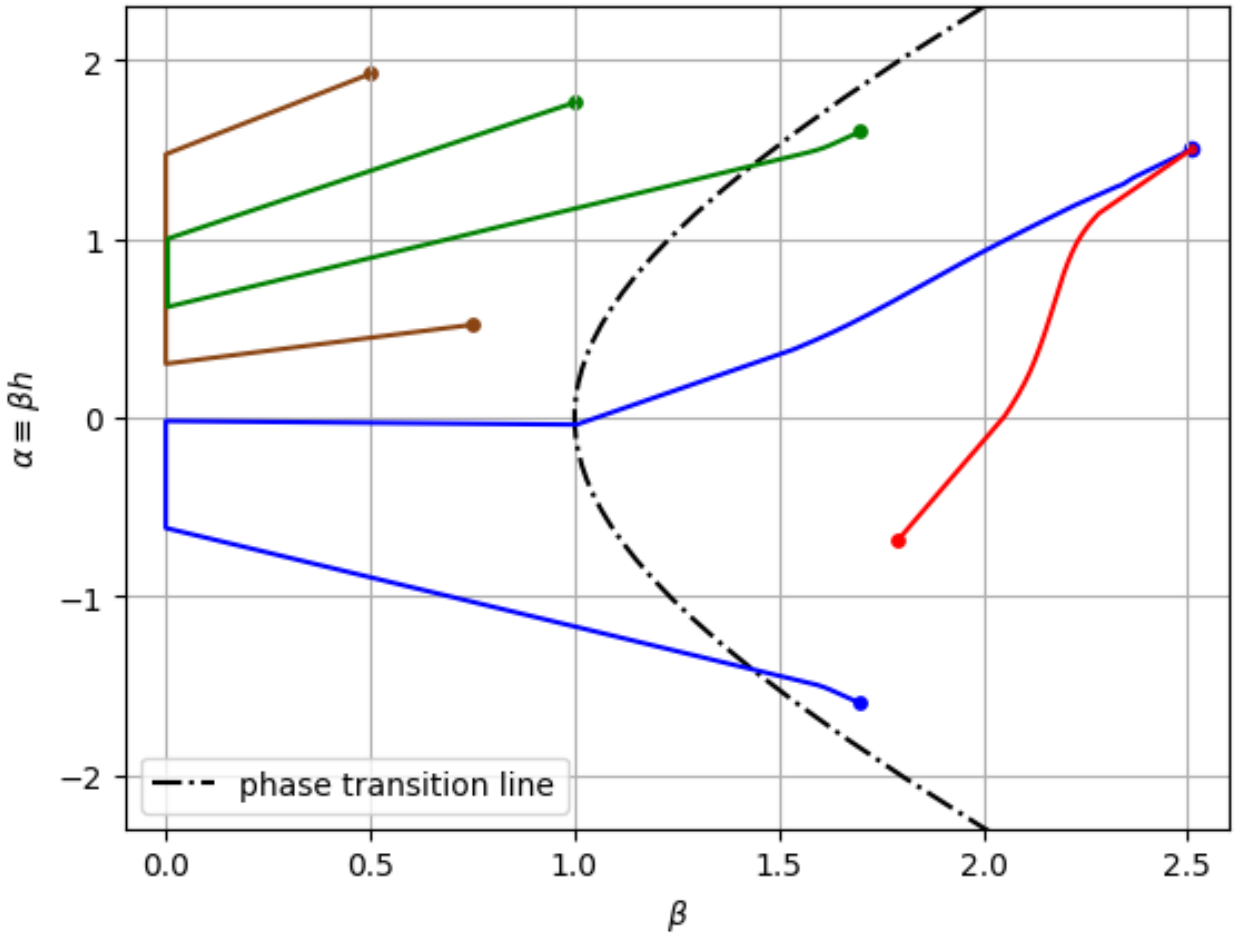

FIG. 3: Illustration of the three types of minimal paths in the mean-field antiferromagnet using the Sivak metric.

The thermodynamic lengths within the antiferromagnetic phase were computed using the Fast Marching Method [23], following the approach of Rotskoff in [12]. Minimal paths were obtained by performing gradient descent along the numerically computed distance function. The code is available on github at the link: https://github.com/Omerbass/FMM-Geodesics.

V. DISCUSSION

These results show that thermodynamic geometry remains a meaningful framework even in the presence of second-order phase transitions, provided the appropriate scaling of thermodynamic quantities is taken into

account. Using the scaling and dynamic scaling hypotheses, I demonstrated that while the Ruppeiner and Sivak metrics generally diverge near criticality, the associated thermodynamic lengths can remain finite for a wide range of universality classes. This implies that finite-dissipation protocols exist even across critical points, as long as the effective metric divergence is sufficiently weak.

For the MF antiferromagnet, the analytic structure of both the Ruppeiner and Sivak metrics reveals a singular but integrable behavior. In the disordered phase, both metrics collapse to a one-dimensional manifold with a null direction corresponding to constant magnetization. Geometrically, this indicates that only one independent degree of freedom contributes to dissipation, while motion along the null direction is thermodynamically free. Consequently, the minimal-dissipation protocol in this phase is obtained by projecting the geodesic flow onto the non-degenerate submanifold, leading to a trajectory that approaches the $\beta = 0$ line, i.e., infinite temperature.

In the ordered phase, the divergence of the metric near the phase boundary mirrors the expected critical singularity of the susceptibility. However, consistent with the scaling analysis, the corresponding thermodynamic length remains finite, suggesting that criticality increases local dissipation rates without rendering finite-time driving impractical. Numerically computed minimal paths confirm this picture: depending on the relative positions of the initial and final states, the shortest path may cross the phase transition or remain within a single phase. Crossing becomes advantageous whenever the direct path between phases is shorter than circumventing the divergent region, reflecting a competition between geometric curvature and metric magnitude.

Altogether, these findings clarify how thermodynamic geometry can be extended to systems exhibiting phase transitions. Even though the metric diverges at criticality, the geometric length—and therefore the minimal excess dissipation—often remains finite, preserving the predictive power of the geometric framework. This result establishes a foundation for optimizing nonequilibrium control in systems with critical points, where the interplay of geometry and dynamics determines the most efficient thermodynamic pathways.

Outlook: Future work could extend this framework to practical systems such as finite-time heat engines operating near criticality [24, 25], where enhanced response functions may either amplify or suppress dissipation. A natural next step is to generalize the geometric approach to first-order phase transitions, where discontinuities in the order parameter introduce new challenges for defining continuous thermodynamic metrics. A systematic study of convergence properties and dissipation bounds would further clarify the limits of validity of the geometric formalism. In particular, the mathematical framework is expected to break down either through the failure of linear-response theory or due to finite-size effects. Establishing quantitative cutoffs for the onset of these regimes would illuminate the interplay between these two limiting factors and may allow for extending the usefulness of the formalism to lower-dimensional systems.

VI. ACKNOWLEDGMENTS

I would like to thank my advisor, Prof. Oren Raz, for his guidance, insight, and encouragement throughout this work. I am grateful to the members of our research group, in particular to Doron Benyamin and Roi Holtzman, for their stimulating discussions, constructive feedback, and continuous support. I am also thankful to David Sivak, and Grant Rotskoff for their valuable contributions and for enlightening conversations that helped shape study.

---

[1] J. W. Gibbs, A method of geometrical representation of the thermodynamic properties of substances by means of surfaces (Longmans, Green and co., 1873) pp. 382–404.

[2] G. Ruppeiner, Thermodynamics: A Riemannian geometric model, Physical Review A **20**, 1608 (1979).

[3] F. Weinhold, Metric geometry of equilibrium thermodynamics, The Journal of Chemical Physics **63**, 2479 (1975).

[4] P. Salamon, J. Nulton, and E. Ihrig, On the relation between entropy and energy versions of thermodynamic length, The Journal of Chemical Physics **80**, 436 (1984).

[5] P. Salamon and R. S. Berry, Thermodynamic Length and Dissipated Availability, Physical Review Letters **51**, 1127 (1983).

[6] B. Andresen, Current Trends in Finite-Time Thermodynamics, Angewandte Chemie International Edition **50**, 2690 (2011).

[7] D. A. Sivak and G. E. Crooks, Thermodynamic Metrics and Optimal Paths, Physical Review Letters **108**, 190602 (2012).

[8] G. E. Crooks, Measuring Thermodynamic Length, Physical Review Letters **99**, 100602 (2007).

[9] G. M. Rotskoff, G. E. Crooks, and E. Vanden-Eijnden, Geometric approach to optimal nonequilibrium control: Minimizing dissipation in nanomagnetic spin systems, Phys. Rev. E **95**, 012148 (2017).

[10] H. Janyszek and R. Mruga la, Riemannian geometry and the thermodynamics of model magnetic systems, Physical Review A **39**, 6515 (1989).

[11] D. Brody and N. Rivier, Geometrical aspects of statistical mechanics, Phys. Rev. E **51**, 1006 (1995).

[12] G. M. Rotskoff and G. E. Crooks, Dynamic Riemannian Geometry of the Ising Model, Physical Review E **92**, 060102 (2015), arXiv:1510.06734 [cond-mat].

[13] H. B. Callen, *Thermodynamics and an introduction to thermostatistics* (Wiley, New York, NY, 1985).

[14] M. Kardar, *Statistical Physics of Fields* (Cambridge University Press, Cambridge, 2007).

[15] U. C. Täuber, *Critical Dynamics: A Field Theory Approach to Equilibrium and Non-Equilibrium Scaling Behavior*, 1st ed. (Cambridge University Press, 2014).

[16] M. D. Kruskal, Maximal extension of schwarzschild metric, Phys. Rev. **119**, 1743 (1960).

[17] G. Szekeres, On the singularities of a Riemannian manifold, Publ. Math. Debrecen **7**, 285 (1960).

[18] J. Cardy, *Scaling and Renormalization in Statistical Physics*, Cambridge Lecture Notes in Physics (Cambridge University Press, 1996).

[19] P. C. Hohenberg and B. I. Halperin, Theory of dynamic critical phenomena, Reviews of Modern Physics **49**, 435 (1977).

[20] G. Odor, Universality classes in nonequilibrium lattice systems, Reviews of Modern Physics **76**, 663 (2004), arXiv:cond-mat/0205644.

[21] E. Vives, T. Castán, and A. Planes, Unified mean-field study of ferro- and antiferromagnetic behavior of the Ising model with external field, American Journal of Physics **65**, 907 (1997).

[22] I. Klich, O. Raz, O. Hirschberg, and M. Vucelja, Mpemba Index and Anomalous Relaxation, Physical Review X **9**, 021060 (2019).

[23] R. Kimmel and J. A. Sethian, Computing geodesic paths on manifolds, Proceedings of the National Academy of Sciences **95**, 8431 (1998).

[24] A. G. Frim and M. R. DeWeese, Geometric bound on the efficiency of irreversible thermodynamic cycles, Phys. Rev. Lett. **128**, 230601 (2022).

[25] M. Campisi and R. Fazio, The power of a critical heat engine, Nature communications **7**, 11895 (2016).